

Design of a custom wideband camera for MISTRAL imager-spectrograph

Eduard R. Muslimov^{a,b}, Jerome Schmitt^c,
Christophe Adami^b, Michel Dennefeld^d,
Marc Ferrari^{b,c}

a–Department of Physics, University of Oxford,
Keble Rd, OX14 3RH Oxford, UK

b–Aix Marseille Univ, CNRS, CNES, LAM, Marseille, France

c–Observatoire de Haute-Provence, Universite d’Aix-Marseille, CNRS,
04870 St-Michel L’Observatoire, France

d–CNRS, Inst. d’Astrophysique de Paris (IAP) and
Sorbonne Université (Paris 6),
98bis, Boulevard Arago, 75014 Paris, France

October 3, 2024

Abstract

MISTRAL is a visible and near infrared imager and spectrograph working with the 1.93m telescope at L’Observatoire de Haute-Provence. The goal of the present project is to design and build one custom lens covering the entire working band 370 – 1000nm with an enhanced throughput and resolution. The proposed design has the focal length of 100mm with $f/\# = 2$ and consists of 5 lenses with 2 aspheres. It is capable to work in spectroscopy or direct imaging mode with the spectral resolving power up to $R590 - 1675$ or energy concentration of 84% within $\pm 1pix$. The throughput varies from 79to98% in the main band of 400-1000 nm with a commercial AR coating and could be yet improved with a custom one. We also demonstrate that with this image quality can be maintained in a $\leq 10\%$ margin with practically reachable tolerances.

Keywords— wideband camera, imaging, low resolution spectroscopy, lens design, visible and near infrared astronomy

1 Introduction

Multi-purpose InSTRument for Astronomy at Low-resolution (MISTRAL) is a visible and near infrared EFOSC type imaging spectrograph developed for the 1.93m telescope at l’Observatoire de Haute Provence [1]. It was developed to cover such science cases as:

- Follow-up of large variable sky surveys, both current and coming (e.g. Vera C. Rubin Telescope[2] and SVOM[3] missions),
- Gamma-ray bursts follow-up,
- Classification of supernovae,
- Study of luminous blue variables, or the numerous peculiar binaries,
- Photometric and spectroscopic studies of objects, already represented in catalogues, but missing resolution or spectral coverage (especially in the high-latitude regions), etc.

MISTRAL has been commissioned in 2021 can be operated in two modes: regular observing runs in visitor mode, and target of opportunity mode with service observing for fast transients

Historically and mainly for the cost reasons, the instrument uses a number of commercial components. In particular, it uses to interchangeable commercial objective lenses to cover the full spectral working range. Namely, Nikkor 105mm f/1.4[4] lens is used for the visible (VIS) part and a Schneider 100mm f/2.9[5] lens for the near infrared (NIR) range of 600-1000 nm. This therefore implies a manual change of the objective according to the wavelength range of interest. Another issue is that the Schneider lens has a smaller aperture, which causes both obscuration and field vignetting. Finally, these lenses are not optimized to work at the edges of the instrument spectral range, so they may under-perform in terms of both throughput and aberrations.

Therefore the goal of current work is to develop a custom camera lens for MISTRAL covering the whole 400-1000 nm band at once in either imaging, VIS spectroscopic or NIR spectroscopic modes. It should have 100 mm focal length and $f/\# = 2$ aperture to match the incoming beam. The required imaging quality is defined by the detector – the instrument uses Andor ikon-L CCD camera with $2048 \times 2048 \times 13.5\mu m$ pixels. So, the lens resolution should be below this value.

The objective lens transmission should be maximized in the working region and, if possible, should allow to extend it in the shortwave direction below 400 nm. Below we consider the general optical design of such a camera, demonstrate its performance and compare it with the commercial lenses currently in use and also show the technological feasibility of the design.

2 Camera optical design

2.1 Nominal design

The camera lens under consideration is installed after the intermediate pupil in the spectrograph coupled with 1.93-m telescope. The general view of the full optical system is shown below in Fig. 1. Note, that there are 2 grisms, which can be mounted in position 7, forming low resolution spectra with reciprocal linear dispersion of $\approx 15\text{nm/mm}$ in the sub-ranges of 400-800 and 600-1000 nm, respectively. Alternatively, an empty diaphragm can be mounted in this position, thus implementing an imaging mode.

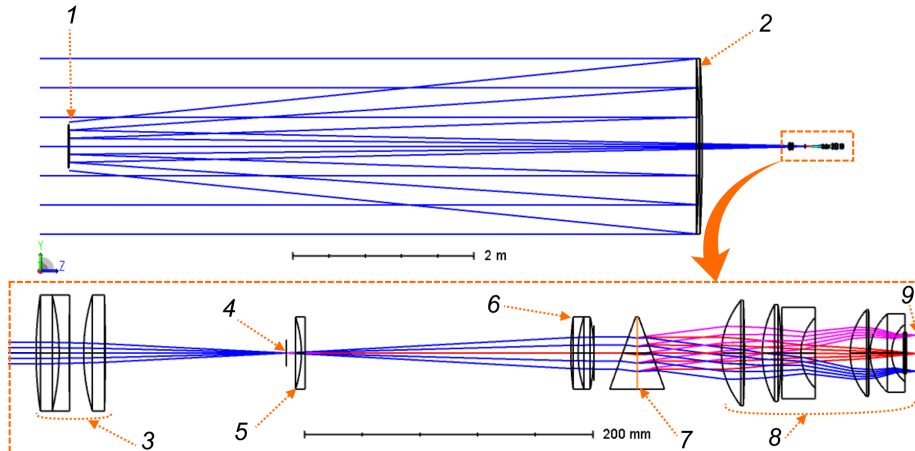


Figure 1: General view of the instrument optical design: 1 – telescope primary mirror, 2 – secondary mirror, 3 – focal reducer lenses, 4 – focal plane/ entrance slit, 5 – field lens, 6 – spectrograph collimator, 7 – grism, 8 – camera lens, 9 – spectral image plane.

The custom lens design used a well-known wide-band triplet design as a starting point. Additional lenses were introduced to reach the required $f/\#$. Cemented

surfaces are excluded to simplify the manufacturing and assembly. Further, 6th order even aspherical surfaces were introduced on the first and the last surface, which are found to be the optimal aspheres positions. Finally, the starting -point design was based on CaF_2 as it has low dispersion and high transmission in a wide spectral band. However, this material is expensive and difficult to polish, especially in a case of fast positive lenses, because of its' brittleness. Therefore it was replaced by S-FPL53 glass from OHARA catalogue (see positive lenses L1,2L2 and L4). The remaining 2 meniscus lenses are made of N-KZFS11 and LAK16A from Schott catalogue, respectively.

The aspherical surfaces shapes is shown as a deviation from the best fit sphere (BFS) in Fig. 2. The first surface on panel "A" has $R_{BFS} = 54.29mm$ and the root-mean square (RMS) deviation of $117.5\mu m$. The last surface in panel "B" has $R_{BFS} = 26.73mm$ and the RMS deviation $69.4\mu m$. These values may be challenging, but reachable with the currently available technologies[6].

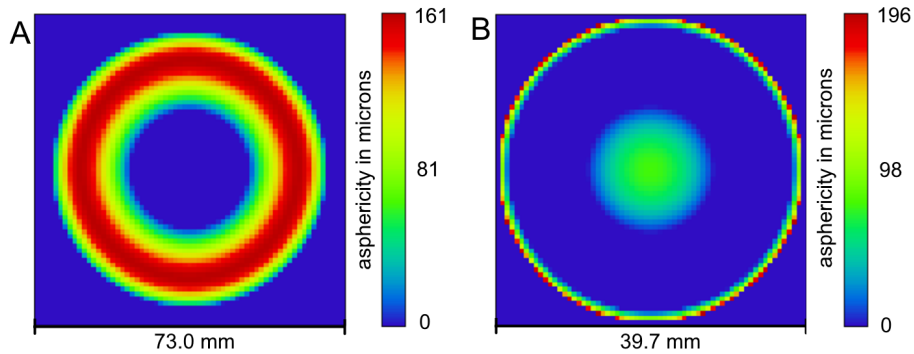


Figure 2: Surface shape deviation from the best fit sphere: A – lens 1, surface 1, B – lens 5 surface 2.

2.2 Optical performance

The geometrical spot diagrams RMS radii were used as the optimization target as the simplest option. So, the first image quality estimation is performed with the spot diagrams. The diagrams in the imaging mode for a lens coupled with the telescope optical system and and the collimator are shown in Fig. 3. The box corresponds to a 4×4 pixels area. The numerical values characterizing the geometrical aberrations are also shown in Table 2 below.

However, the geometrical spots do not provide a correct understanding of the energy distribution in the image. So, we extract the ensquared energy diagrams,

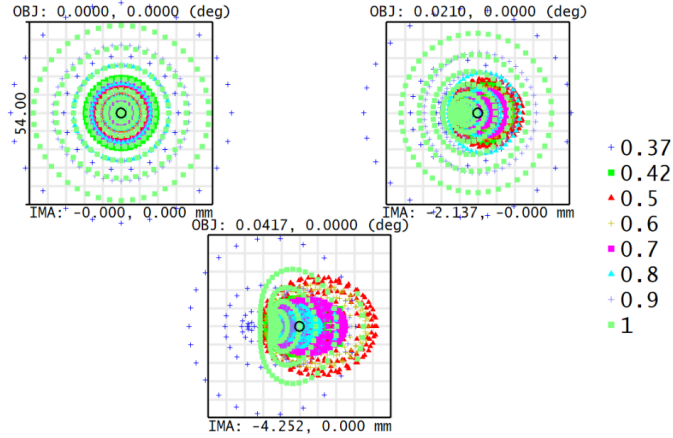


Figure 3: Polychromatic spot diagrams in the imaging mode at 4 pixels scale.

corresponding to 2×2 and 4×4 are - see Fig. 4. Similarly, the key numerical values are summarized further in Table 2.

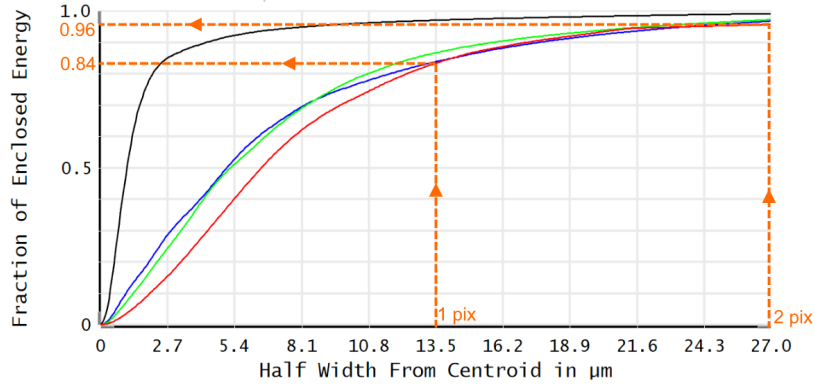


Figure 4: Ensquared energy in polychromatic PSF in the imaging mode, compared to 1 and 2 pixels radial distance.

For the spectral imaging performance we compute the instrument functions, which represent a convolution of the entrance slit brightness distribution and the spectrograph line spread function (LSF) in the dispersion plane. The slit brightness is supposed to be uniform in this case. In practice it may differ from this

simple shape significantly depending on the object type, atmospheric turbulence etc. However, this should be enough for a comparative study. The Instrument functions for the field centre and edge are shown in Fig. 5.

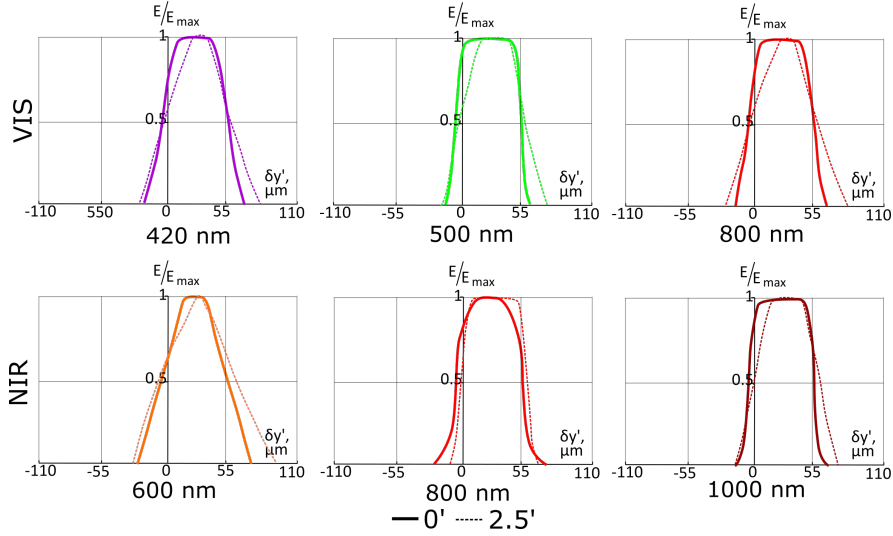


Figure 5: Spectrograph instrument functions in spectral modes with the custom camera lens (geometrical slit image width is $56\mu m$).

These instrument functions are computed for the geometrical width of the slit image on the detector equal to $56\mu m$ or 4 pixels. It is clear that with this slit the spectral resolution doesn't reach the limits set by the detector and spectrograph's optics. So we consider an alternative case of $40\mu m$ slit, which may be implemented in practice after the instrument upgrade and installation a variable width slit. Spectral resolving power, defined by the instrument function's full width at half maximum (FWHM) and the reciprocal linear dispersion $R = \frac{\lambda}{FWHM d\lambda/d\lambda}$ is presented in Table 3 for both of these cases.

Finally, one of the main reasons behind the development of new camera is its' throughput. With a 5 lens design it becomes possible to reach relatively high transmission even with standard anti-reflection (AR) coatings. For example, a coating equivalent to AB type from Thorlabs[7] allows to reach $> 90\%$ average transmission for the most of the working range, although it drops sharply at the shortwave edge - see solid curve in Fig. 6. Alternatively, we can consider a customized coating covering the entire waveband. Even a moderate residual reflectivity of $\rho \leq 1\%$ would provide a high and uniform overall transmission - see the dashed curve in Fig. 6.

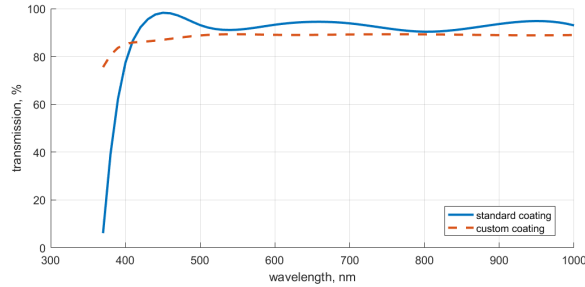


Figure 6: Spectral dependence of the custom lens transmission with 2 types of AR coating.

2.3 Tolerances estimations

In the sake of simplicity we use the geometric aberrations to perform the tolerance analysis. In particular, we set an increase by 10% of the spot diagram RMS radius as the target image quality criterion. Then we perform a standard sensitivity and tolerances analysis for the direct imaging mode, as its' image quality correlates well with that in the spectral modes. The set of variables is typical for a lens design analysis. It should be noted that the aspheres are sensitive to centering and linear decenter is not equivalent to a tilt for them. Finally, only the back focus is used as a compensator. The results are shown in Table 1 below in a short form, i.e. only the extreme values per category are specified. Some of these tolerances may be challenging and could require some additional facilities during the manufacturing and alignment, but in general this level of precision is reachable[8].

3 Performance comparison

First of all, the custom design described above has is superior over the commercial NIR lens as it passes the entire science beam without cropping or field vignetting. Fig. 7 visually illustrates the geomteric transmissison gain.

Further, in order to quantify the performance gain reachable with the custom lens, we perform the same computations for the spectrograph equipped with the commercial lenses.

The difference of resolution in direct imaging mode is shown in the summary Table 2. Both the sopt diagram-based metrics and ensquared energy values are shown here. As one can see, in comparison with the Nikkor VIS lens, the proposed design has larger spot wings, but in general the resolution is more uniform over

Table 1: Minimum and maximum tolerances values for each category.

Tolerance	Min	Max
Radius , finges @589 nm	-	5
Thickness , μm	15	100
Element decenter, μm	15	200
Element tilt,'	0.9	11
Aspheres decenter, μm	15	28
Surface tilt,'	0.6	6
Surface irregularity, nm	-	68.3
Refraction index	2×10^{-4}	1×10^{-3}
Abbe number	0.147	0.95

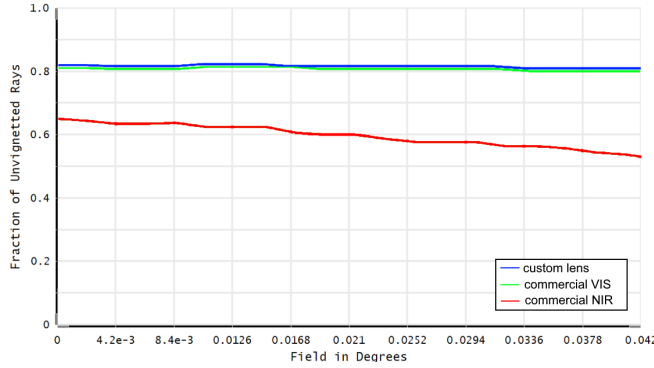


Figure 7: Comparison of vignetting and central obscuration in the ”telescope + spectrograph” optical system with different camera lenses.

the field. Note, that each time only the nominal waveband is used for simulations, so the chromatism correction for the VIS lens was simpler. At the same time the custom design is superior over the commercial NIR lens regardless of the metric or reference point.

In a similar way, the spectral resolving power for each camera lens are shown in table 3 to table 5. Using the custom lens has a minor effect because of the slit oversampling mentioned before. With the current slit width it provides a modest $\approx 4\%$ growth of the resolution for a part of NIR spectrum. However, changing the entrance slit may unlock the camera potential and would allow to reach a factor

Table 2: Resolution metrics for undispersed image

Metric	Custom-designed lens		Commercial VIS		Commercial NIR	
	$\omega = 0$	$\omega = 2.5'$	$\omega = 0$	$\omega = 2.5'$	$\omega = 0$	$\omega = 2.5'$
RMS spot rad., μm	9.2	9.9	13.3	11.1	17.9	23.0
PTV spot rad., μm	32.6	32.6	25.6	25.1	44.8	75.2
Esquared energy $r \leq 13.5\mu m$	86%	84%	92%	74%	61%	59%
Esquared energy $r \leq 27\mu m$	97%	96%	99%	99%	91%	86%

of 1.57 gain in some cases.

Table 3: Spectral resolving power with custom lens.

λ, nm	$\omega = 0,$ $y' = 56\mu m$	$\omega = 2.5',$ $y' = 56\mu m$	$\omega = 0,$ $y' = 40\mu m$	$\omega = 2.5',$ $y' = 40\mu m$
370	438	438	613	590
420	497	497	696	696
500	592	592	829	768
800	947	947	1326	896
600	718	665	1005	1005
800	947	957	1340	1340
1000	1184	1197	1675	1675

The next metric to compare is the lens transmission. The comparison ignores the geometric vignetting factors discussed before. For the custom lens we use the standard AR coating data (see Fig. 6). For the commercial VIS lens we do not have the exact data, so we have to presume the number of surfaces using the closest known design[9] and some residual reflection of the AR $\rho \leq 1\%$. In turn, for the

Table 4: Spectral resolving power with commercial VIS camera.

λ, nm	$\omega = 0,$ $y' = 40\mu m$	$\omega = 2.5',$ $y' = 40\mu m$
370	-	-
420	497	497
500	592	592
800	947	947

Table 5: Spectral resolving power with commercial NIR camera.

λ, nm	$\omega = 0,$ $y' = 40\mu m$	$\omega = 2.5',$ $y' = 40\mu m$
600	718	641
800	947	957
1000	1139	1197

NIR lens the data is known from its' official specifications[5]. As the table shows, the custom lens is better or comparable in terms of transmission for the most of the waveband and has a significant advantage at the shortest wavelengths.

Finally, to visualize the advantages of the proposed new camera design, we simulate an image of extended celestial object. We use an image of "Bug Nebula" (Planetary Nebula NGC 6302) for this purpose. It has an angular size of $1.8'$, which is representative for our nominal field of $\pm 2.5'$. We use the wavelengths $\lambda = 420, 600$ and $800nm$ covering the VIS range instead of the RGB triplet to generate false-colour images. The gain in resolution is clear in fine details of the simulated images.

4 Conclusions and future work

In the present paper we proposed a custom camera lens for the MISTRAL spectrograph and imager at 1.93m telescope at OHP. It is shown that this design has significant advantages in terms of throughput and resolution in the direct imaging and long-slit spectroscopy modes. At the same time, the optical design, including the nominal parameters and the tolerances, is technologically feasible.

Table 6: Lens throughput and resolution comparison

Wavelength, nm	Custom-designed lens	Commercial VIS	Commercial NIR
400	77.4%	18.6%	52%
500	93.1%	72.5%	92%
600	93.3%	74.7%	93%
700	93.8%	75.2%	93%
800	90.3%	n/a	95%

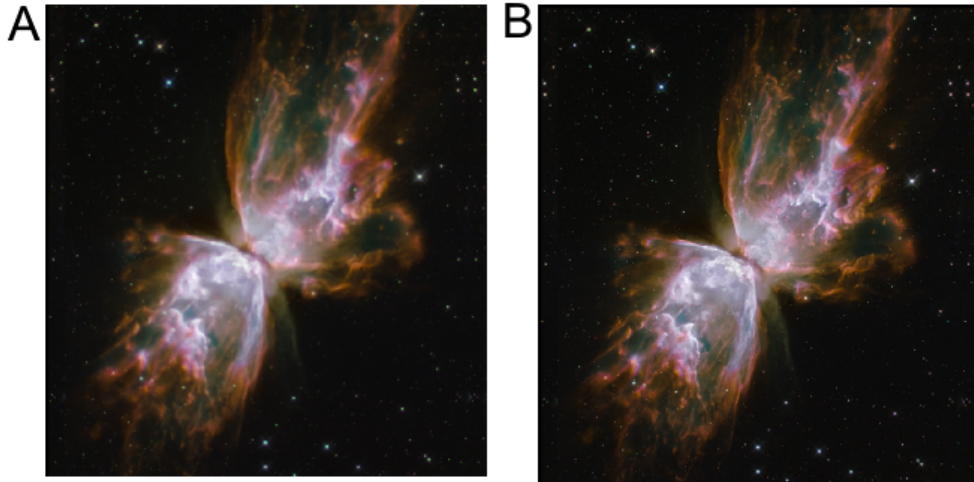


Figure 8: Comparison of simulated images of Bug Nebula: A – commercial Nikon lens, B – custom camera lens.

The next stages of the project should include development of the opto-mechanical design, which would provide the required accuracy and stability and coupling with the existing interface of Andor camera. The latter point may require some additional effort as the back focal length is shorter than that of the commercial lenses used at the moment. Once the opto-mechanical design is ready, we could proceed to manufacturing, alignment test and installation of the new camera. A simultaneous upgrade of the entrance slit unit would help to maximize the gain in terms of spectral resolving power.

ACKNOWLEDGMENTS

Authors thank the CPER OHP2020 Region Sud and the Conseil departemental des Alpes de Haute Provence for their contribution. This research has also made use of the MISTRAL database, operated at CeSAM (LAM), Marseille, France. This work received support from the French government under the France2030 investment plan, as part of the initiative d’Excellence d’Aix- Marseille Universite-A*MIDEX (AMX-19-IET-008). We were also supported by the IPhU Graduate School program at Aix-Marseille University. EJ is a FNRS Senior Research Associate. We also acknowledge the support by Master Erasmus Mundus Europhotonics (599098-EPP-1-2018-1-FR-EPPKA1-JMD-MOB) financed by EACEA (European Education and Culture Executive Agency). Authors thank the CNES for financial support of the MISTRAL operations.

References

- [1] J. Schmitt, C. Adami, and M. D. et al., “Multi-purpose instrument for astronomy at low-resolution: Mistral@ohp,” 2024.
- [2] R. L. Jones, M. T. Bannister, B. T. Bolin, and et al., “The Scientific Impact of the Vera C. Rubin Observatory’s Legacy Survey of Space and Time (LSST) for Solar System Science,” *Bulletin of the AAS*, vol. 53, mar 18 2021. <https://baas.aas.org/pub/2021n4i236>.
- [3] M. G. Bernardini, B. Cordier, and J. Wei, “The svom mission,” *Galaxies*, vol. 9, no. 4, 2021.
- [4] Nikon, “Fx af-s nikkor 105mm f/1.4.” <https://www.nikon.co.uk>.
- [5] Schneider, “Emerald 2.9/100 f-ld.” <https://schneiderkreuznach.com>.
- [6] A. Beutler, “Metrology for the production process of aspheric lenses,” *Advanced Optical Technologies*, vol. 5, no. 3, pp. 211–228, 2016.
- [7] Thorlabs, “Optical coatings.” <https://www.thorlabs.com/>.
- [8] P. Langehanenberg, J. Heinisch, C. Buß, and C. Wilde, “High-precision mounted lens production,” *Optik & Photonik*, vol. 9, no. 2, pp. 41–45, 2014.
- [9] T. Uzawa, N. Fujii, and A. Ishii, “Zoom lens,” June 13 1996. US Patent 5,572,277A.